Spectrum Cartography Based on Dynamic Compressed Sensing by Using Multiple Domains Information

Haiyang Xia, Song Zha, Jijun Huang, Jibin Liu, and Peiguo Liu

***Abstract*—Radio maps have experienced their success in applications of wireless communications for years by offering metrics of radio frequency (RF) information, e.g., power spectral density (PSD), within a geographical region of interest. Spectrum cartography technique constructs radio maps to expand the abilities of RF awareness. However, seldom of existing methods aim at constructing radio maps by utilizing multiple domains information. In this paper, a novel framework inspired by dynamic compressed sensing (DCS) has been proposed firstly to solve this problem. This flexible framework first to apply joint group-Lasso for PSD map construction based on the different sparse patterns between space and frequency domains as well as innovatively utilizes transmitters' mobility patterns for support prediction of DCS. Simulation experiments have been processed to assess the performance of methods within the proposed framework and framework's superiority has been proven.**

***Index Terms*—DCS, group-Lasso, PSD, sparsity, spectrum cartography, support prediction.**

I. Introduction

SPECTRUM cartography [1], [2] has been introduced to construct radio maps [3], [4] of a certain channel metric [5], such as power spectral density (PSD), received signal power (RSS) or channel gain over a geographical region of interest based on measurements collected by the radio frequency (RF) sensors deployed within the region [1] for years. Since radio maps comprise the critical information [6], [7] of RF environment across multiple domains [8], e.g., space, frequency, and time, they have been widely utilized in applications of wireless communications including network planning, interference coordination, dynamic spectrum access, and spectrum surveillance. Meanwhile, the PSD map [9]–[11] has become one of the most popular forms of radio maps.

Due to the prosperous development of mobile transmitters, radio maps also find applications in mobile wireless communications, such as intelligent transport system (ITS) for autonomous vehicles (AVs) or unmanned aerial vehicles (UAVs)-based networks [12]–[14]. Unlike conventional wireless communication devices, their locations are always time-varying, but the mobility patterns are regulated by traffic regulations, e.g., limitations of velocity. These features consist of variance or invariance of space domain sparsity and frequency domain sparsity, which reveals the changing rules of RF environment with time lapse.

For the scenario of non-cooperative transmitters, existing construction methods of radio maps process the estimation of signal power or any other electromagnetic physical quantities at one time slot, at any arbitrary locations within region of interest, based on the related measurements without prior information. These dominating methods include but not limit to interpolation [15], [16] or extrapolation and their revised algorithms [17], [18], semi-parameter regression [19], matrix completion [20], kernel-based learning [21], and dictionary learning [22]. These methods are effective to a certain extent, but challenges still remain. Most of them construct power maps without consideration of connection between space and frequency domains.

In order to construct PSD maps, some methods [23], [24] have been proposed to exploit the spatial sparsity inspired by theories of compressed sensing (CS) [25], [26]. Another explicit example is that the least-absolute shrinkage and selection operator (Lasso) [27], [28] has been employed to determine the basis expansion model (BEM) coefficients [29], [30] for PSD estimation [31], [32]. Moreover, the group-Lasso [33] also has favorable performance in spectrum cartography [34], and most of them adopt basis pursuit (BP) [35] as basic approach for CS problem. Nevertheless, these methods also construct PSD maps at each time slot individually, which means they ignore temporal varying rules of space and frequency domains. And approaches based on dynamic compressed sensing (DCS) can be employed to address this limitation.

The majority of DCS reconstruction methods can be classified into two categories: those based on least squares [36] and those based on Bayesian prediction [37], [38]. The former one makes the temporal prediction through analysis of support (the sequence of nonzero entries in the sparse vector) variation according to the prior information offered by time-varying patterns of support, including the least square compressed sensing (LS-CS) [39], the Kalman filter compressed sensing (KF-CS) [40], modified-DCS [41], modified orthogonal matching pursuit (modified-OMP) [42], weighted- and so on. Differently, the latter one aims at the prediction of posterior probability by the prior probability of parameters of random variables as well as the likely probability formed by compressed observation matrix [38], [43]. But the prior distribution

Manuscript received July 19, 2022 revised June 24, 2023; approved for publication by Sangheon Pack, Division 2 Editor, June 26, 2023.

This work was supported in part by the National Natural Science Foundation of China (No. 61601491 and No. U19A2058).

The authors are with the College of Electronic Science and Technology, National University of Defense Technology, Changsha, 410073, China, email: easonhsia@sina.com, zhasong0551@163.com, 1465580012@qq.com, liujibin@gfkd.edu.com, and pgliu@163.com.

S. Zha is the corresponding author.

Digital Object Identifier: 10.23919/JCN.2023.000028

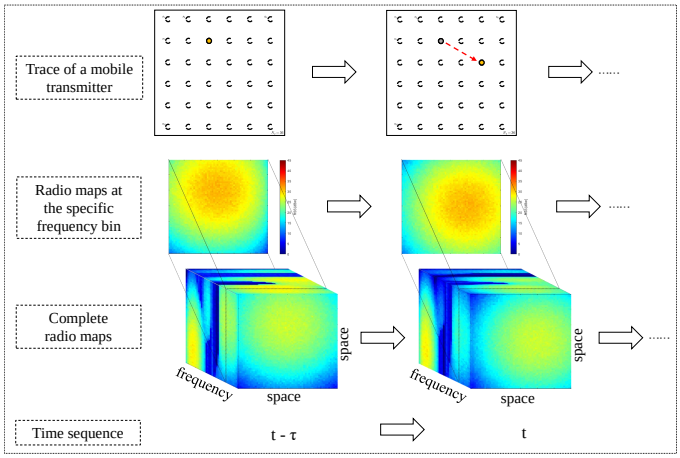

Fig. 1. Illustration of trace of a mobile transmitter, radio maps at the specific frequency bin, and complete PSD maps with time sequence.

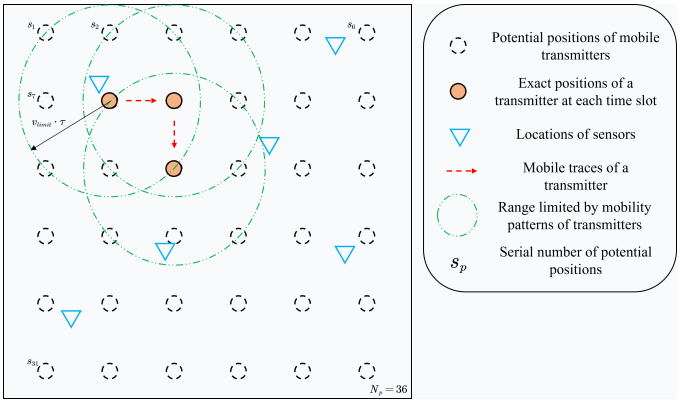

Fig. 2. Virtual network grid of the spatial region of interest.

of random variables' parameters is difficult to access on the condition of complicated wireless communication scenario. In the contrary, the ideas of research on the variation of support are worth reference to fit for the dynamic scenario discussed above, so we choose them for highly accurate PSD estimation. However, the BEM coefficients of PSD in our scenario do not follow two basic assumptions [36], "slow support change" and "slow signal value change", the approaches mentioned above cannot be utilized in the scenario of mobile transmitters directly.

To this end, a novel DCS framework based on the utilization of multiple domains information has been put forth for PSD maps construction in this paper. This framework applies joint group-Lasso based on different sparse patterns of space and frequency domains as well as DCS support prediction based on temporal varying rules of space and frequency domains. Its estimation can be organized to construct complete PSD maps in the time sequence, see Fig. 1. The performance of methods within the proposed framework have been compared by numerical experiments. In addition, both the normalized vector errors (NVE) [32] and the spatial-frequency power overlap ratio (SFPOR) have been employed to verify PSD estimation accuracy.

The main contributions of this work include: (i) it innovatively utilizes history information of estimations and mobility patterns (e.g., velocity limitation in this paper discussed latter) of mobile transmitters to reveal temporal varying rules of space and frequency domains for DCS support prediction; (ii) it firstly applies joint group-Lasso with different plenty items according to difference analysis of space and frequency domains; (iii) it also firstly propose a flexible framework for PSD maps construction, for it can adjust the approach depending on whether history information of estimation or transmitters' mobility patterns are provided or not.

The rest of the paper has been organized as follow. Section II describes the system model and problem statement. In Section III, joint group-lasso (JG-Lasso) based on different sparse patterns, lasso of temporal space-frequency support prediction (TSFP-Lasso) and joint group-lasso of temporal space-frequency Support prediction (TSFP-JG-Lasso) have been illustrated in details. Experiment setting and results analysis are represented in Section IV while conclusions of the paper are drawn in Section V.

Notation: Bold uppercase $\mathbf{A}$ (lowercase $\mathbf{a}$) letters denote matrices or tensors (vectors), A_{ij} denotes the (i,j)th entry of matrix $\mathbf{A}$, a_i denotes the ith entry of vector $\mathbf{a}$, $\mathbf{A}_{i:}$ denotes the ith row sub-vector of matrix $\mathbf{A}$ while $\mathbf{A}_{:j}$ denote the jth column sub-vector of matrix $\mathbf{A}$, $\mathbf{A}^\top$ is the transpose of matrix $\mathbf{A}$, Δ is the support set of vector, $\mathbf{A}^\Delta$ denotes the Δ columns of matrix $\mathbf{A}$, $\mathbf{a}_\Delta$ denotes the Δ entries of $\mathbf{a}$, Δ^C denotes the completement of set Δ, $\hat{\mathbf{a}}(t)$ is the final estimation of vector $\mathbf{a}$ at time slot t, and $\check{\mathbf{a}}(t)$ is the pre-estimation of vector $\mathbf{a}$ only based on measurements at time slot t.

II. System Model and Problem Statement

A. Network Model

Consider N_p potential positions of mobile transmitters, between which is the reference distance d_{ref}, and N_m sensors receiving and measuring the signal power in a geographical region $\mathcal{R} \subset \mathbb{R}^2$, portraited in Fig. 2. With the collection of known bases $\{\beta_q(f)\}_{q=1}^{N_q}$, where the basis $\beta_q(f)$ is centered at frequency f_q, the PSD of pth mobile transmitters' emission $\varphi_p(f)$ can be denoted as

$$\varphi_p(f) = \sum_{q=1}^{N_q} \varsigma_{pq}\beta_q(f), p = 1, 2, \cdots, N_p, \tag{1}$$

where ς_{pq} denotes the expansion coefficient belongs to each base, awaiting to be estimated to construct the PSD map [31]. Among those basis models, the Gaussian bells $\beta_q(f) = \exp\left[-(f - f_q)^2\right]$ are deployed with center frequencies equispaced on the bandwidth B of interest.

B. Propagation Model

Then, consider a deterministic pathloss model for the signal propagation from mobile transmitters to sensors within the region of interest, and the signal power is scaled by a mask matrix with entries $\gamma_{pm} = \exp\left(-\eta \|s_p - s_m\|_2^2\right)$, where η denotes pathloss coefficients controlling the attenuation per

reference distance, $\{s_p\}_{p=1}^{N_p}$ and $\{s_m\}_{m=1}^{N_m}$ denote the position vectors of potential mobile transmitters' position and sensors deployed by ITS, respectively. It is worth stressing that this mask matrix reflects the known information of gain in the propagation environment. Although the selection of signal propagation must be chosen accordingly based on different environments, it has little influence on the performance of methods in this paper as known information. For simplicity and generality, the exponential signal model is chosen in this paper as [32].

Therefore, the power measured by the mth senor can be expressed by the superposition of signal power transmitted by each potential mobile transmitters' positions plus the Gaussian white noise, as

$$\begin{aligned}\varphi_m(f) &= \sum_{p=1}^{N_p} \gamma_{pm}\varphi_p(f) + \sigma_m^2, m = 1, 2, \cdots, N_m \\ &= \sum_{p=1}^{N_p} \gamma_{pm} \sum_{q=1}^{N_q} \varsigma_{pq}\beta_q(f) + \sigma_m^2,\end{aligned} \tag{2}$$

where σ_m^2 denotes the noise power.

Furthermore, the expansion coefficients $\{\varsigma_{pq}\}$ are estimated based on the measurements collected by N_m sensors using N_l frequency samples on each time slot t, the PSD of the region of interest can be denoted as

$$\Xi(\boldsymbol{s}, f, t) = \sum_{p=1}^{N_p}\sum_{q=1}^{N_q} \varsigma_{pq}(t)\gamma_p(\boldsymbol{s})\beta_q(f),$$

where $\boldsymbol{s}$ denotes the vector at any position within the region, and (2) can be revised as

$$\varphi_{ml}(t) = \sum_{p=1}^{N_p} \gamma_{pm} \sum_{q=1}^{N_q} \varsigma_{pq}(t)\beta_q(f_l) + \sigma_m^2, \tag{3}$$

where $\varphi_{ml}(t)$ denotes the lth frequency sample of signal power measured by mth sensor at time slot t. Moreover, (3) can also be rewritten in matrices form as

$$\varphi_{ml}(t) = \mathbf{b}_m^\top(f_l) \cdot \varsigma(t) + \sigma_m^2, \tag{4}$$

where $\mathbf{b}_m^\top(f_l) = \left[\gamma_{1m}\beta_1(f_l), \cdots, \gamma_{1m}\beta_{N_q}(f_l), \cdots, \gamma_{N_p m}\beta_{N_q}(f_l)\right]^\top$ and $\varsigma(t) = \left[\varsigma_{11}(t), \varsigma_{12}(t), \cdots, \varsigma_{1N_q}(t), \cdots, \varsigma_{N_p N_q}(t)\right]^\top$. And the overall measurements can be expressed as

$$\mathbf{\Phi}(t) = \mathbf{B} \cdot \varsigma(t) + \sigma_m^2 \cdot \mathbf{1}_{N_m N_l \times 1} + e_m, \tag{5}$$

where $\mathbf{\Phi}(t) = [\varphi_{11}(t), \varphi_{12}(t), \cdots, \varphi_{1N_l}(t), \cdots, \varphi_{N_m N_l}(t)]^\top$ denotes N_l frequency samples of N_m sensors, $\mathbf{B} = \left[\mathbf{b}_1^\top(f_1), \mathbf{b}_1^\top(f_2), \cdots, \mathbf{b}_1^\top(f_{N_l}), \cdots, \mathbf{b}_{N_m}^\top(f_{N_l})\right]^\top$ denotes the propagation matrix, and $\mathbf{1}_{N_m N_l \times 1}$ denotes $N_m N_l$-by-1 array of ones.

After the solution of $\varsigma(t)$ at each time slot t, $T(t)$ can be utilized to denote the support of $\hat{\varsigma}(t)$. As for the next time slot $t+\tau$, $\Delta_{mobil}(t+\tau)$ is defined as the possible support based on velocity limitation v_{limit} and $\hat{\varsigma}(t)$, and $T_{pred}(t+\tau)$ is defined as the support prediction of $\varsigma(t+\tau)$ resulted from $\Delta_{mobil}(t+\tau)$ and the pre-solution $\hat{\varsigma}_{pre}(t+\tau)$.

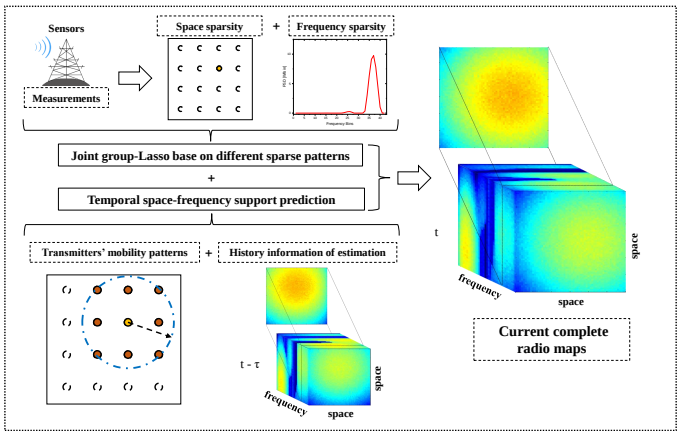

Fig. 3. Illustration of the problem statement.

C. Problem Statement

The objective of this paper is to estimate the dynamic BEM coefficients for PSD maps construction of mobile transmitters within region of interest by the proposed framework, according to the propagation model, current sensor measurements and multiple domains information including different sparse patterns between space and frequency domains and temporal varying rules of space and frequency domains. In other words, our aim is to perform

1) **Joint group-Lasso based on different sparse patterns** Obtain the $\{\varsigma_{JG}(t)\}_{t=1}^{toT}$ based on $\{s_p\}_{p=1}^{Np}$, $\{\beta_q(f)\}_{q=1}^{N_q}$, $\{s_m\}_{m=1}^{N_m}$, $\{f_l\}_{l=1}^{N_l}$, and $\{\mathbf{\Phi}(t)\}_{t=1}^{toT}$.

2) **Lasso of temporal space-frequency support prediction** Estimate $\{\varsigma_{TSFP}(t)\}_{t=1}^{toT}$ based on $\{s_p\}_{p=1}^{Np}$, $\{\beta_q(f)\}_{q=1}^{N_q}$, $\{s_m\}_{m=1}^{N_m}$, $\{f_l\}_{l=1}^{N_l}$, v_{limit}, and $\{\mathbf{\Phi}(t)\}_{t=1}^{toT}$.

III. BEM Coefficients Estimation of PSD

A. Joint Group-Lasso Based on Different Sparse Patterns

According to the model introduced in Section II, the sparsity of $\varsigma(t)$ is obvious because of the uniqueness of each mobile transmitter in space and frequency domains. In other words, only a small fraction of frequency is occupied compared with the whole bandwidth in a few positions of existing active mobile transmitters within the region. And the non-negative least square (NNLS) criterion based on the linear model in (2) can be expressed as

$$\min_{\varsigma \geq 0} \left\| \mathbf{\Phi}(t) - \mathbf{B} \cdot \varsigma(t) - \sigma_m^2 \cdot \mathbf{1}_{N_m N_l \times 1} \right\|^2. \tag{6}$$

The potential positions of mobile transmitters $\{s_p\}_{p=1}^{Np}$ and the locations deployed at sensors $\{s_m\}_{m=1}^{N_m}$ are known, or the NNLS optimization above is rendered non-convex. And Lasso, a.k.a. de-noising basis pursuit [44], has proven its splendid ability in exploiting the sparsity of unknown vectors by augmenting the l_1-norm weighting by a tuning parameter λ, as

$$\min_{\varsigma \geq 0} \left\| \mathbf{\Phi}(t) - \mathbf{B} \cdot \varsigma(t) - \sigma_m^2 \cdot \mathbf{1}_{N_m N_l \times 1} \right\|^2 + \lambda \left\| \varsigma(t) \right\|_1. \tag{7}$$

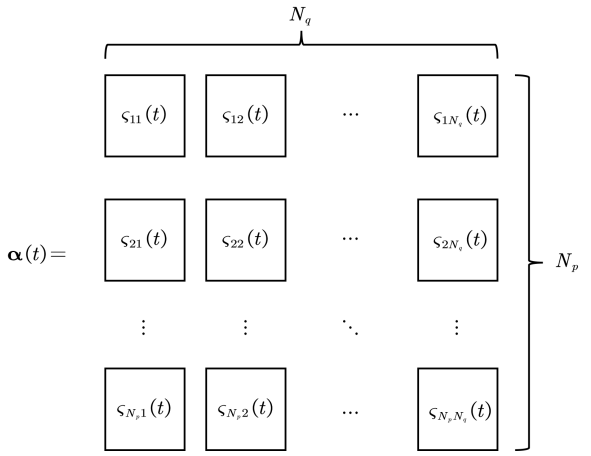

Fig. 4. The composition of $\alpha(t)$.

In consideration of the sparsity in both frequency and space domains, the support of $\varsigma(t)$ tends to be in some specific frequency f_l and exact position s_p. If an l_1-norm penalty is applied to the whole $\varsigma(t)$, Lasso tends to make the selection based on the strength of individual measurement entry instead of the strength of groups of counterparts [33]. That is, if we hope to better exploit the sparsity of signal expansion coefficients, the norm penalty should be applied in every group composed of the $\varsigma(t)$.

However, the sparsity in the frequency domain is different from that in the space domain. To analyze the sparsity distribution in frequency and space domains, the $\varsigma(t)$ can be denoted as

$$\alpha(t)=\left[\boldsymbol{\varsigma}_{1:}{}^{\top}(t),\boldsymbol{\varsigma}_{2:}{}^{\top}(t),\cdots,\boldsymbol{\varsigma}_{N_p:}{}^{\top}(t)\right]^{\top}, \tag{8}$$

where $\boldsymbol{\varsigma}_{p:}{}^{\top}(t)$ is an N_q-by-1 vector of the pth sub-vector of $\varsigma(t)$. That is, rows of the $\alpha(t)$ describe the frequency domain at each s_p, while columns of the $\alpha(t)$ describe the space domain at each f_q, as depicted in Fig. 4.

Following the composition of $\alpha(t)$ within an active CR, the frequency bandwidth is nearly occupied and the PSD of each mobile transmitter's transmission is of the same magnitude, but the spatial positions are hardly fully utilized. For one, it is impossible to fill the whole regional space with mobile transmitters but not including buildings, pedestrians, or other traffic infrastructure, and the carriageway covers just parts of regions. For another, the geographic region is a two-dimension area, just mentioned in Section II, so its continuity cannot be conveyed into a vector, which is a one-dimension carriage, directly and completely.

Because of the difference between frequency and space domain, it is necessary to select the suitable penalty for regularization items of different domain groups. Apart from the l_1-norm from Lasso, the l_2-norm from ridge regression [45] is also a popular choice of penalty item. The former treats entries within groups of $\varsigma(t)$ differently, and this encourages sparsity in each individual entry [27], [46], which fits the spatial distribution. But the latter tends to treat all entries within the same group equally, and this encourages "coupling strength" among group-size entries [45], [46], which better fits the PSD estimation.

Algorithm 1 JG-Lasso of spatial-frequency domain for expansion coefficients estimation

Input: $\{s_p\}_{p=1}^{Np},\{\beta_q(f)\}_{q=1}^{N_q},\{s_m\}_{m=1}^{N_m},\{f_l\}_{l=1}^{N_l},$ $\{\boldsymbol{\Phi}(t)\}_{t=1}^{toT}$
Parameters: $\eta, d_{res}, \lambda_{spa}, \lambda_{freq}$
$\beta_q(f_l)=\exp\left[-(f_l-f_q)^2\right]$
$\gamma_{pm}=\exp\left(-\eta\left\|s_p-s_m\right\|_2^2\right)$
$\mathbf{b}_m^{\top}(f_l)=\left[\gamma_{1m}\beta_1(f_l),\cdots,\gamma_{N_pm}\beta_{N_q}(f_l)\right]^{\top}$
$\mathbf{B}=\left[\mathbf{b}_1^{\top}(f_1),\mathbf{b}_1^{\top}(f_2),\cdots,\mathbf{b}_1^{\top}(f_{N_l}),\cdots,\mathbf{b}_{N_m}^{\top}(f_{N_l})\right]^{\top}$
for $t=1,2,\cdots,toT$ **do**
  Obtain $\hat{\varsigma}(t)$ using (9)
end for
$\{\varsigma_{JG}(t)\}_{t=1}^{toT}$ equals $\{\hat{\varsigma}(t)\}_{t=1}^{toT}$
Output: $\{\varsigma_{JG}(t)\}_{t=1}^{toT}$

Consequently, to cooperate the parsimonious division of group, the l_1-norm is employed as penalty items of the spatial groups while the l_2-norm is employed as penalty items of the frequency groups, (7) can be rewritten as

$$\min_{\varsigma\geq 0}\left\|\boldsymbol{\Phi}(t)-\mathbf{B}\cdot\varsigma(t)-\sigma_m^2\cdot\mathbf{1}_{N_mN_l\times 1}\right\|^2 + \lambda_{spa}\sum_{q=1}^{N_q}\left\|\varsigma_{spa}(q,t)\right\|_1+\lambda_{freq}\sum_{p=1}^{N_p}\left\|\varsigma_{freq}(p,t)\right\|_2, \tag{9}$$

where $\varsigma_{spa}(q,t)=\sum_{p=1}^{N_p}\varsigma_{pq}(t)$, $\varsigma_{freq}(p,t)=\sum_{q=1}^{N_q}\varsigma_{pq}(t)$, λ_{spa} and λ_{freq} are the tunning parameter of each penalty item, respectively. And $\{\varsigma_{JG}(t)\}_{t=1}^{toT}$ equals $\{\hat{\varsigma}(t)\}_{t=1}^{toT}$ of (9).

The algorithm of JG-Lasso of spatial-frequency domain for expansion coefficients estimation is illustrated in **Algorithm 1**.

B. Lasso of Temporal Space-Frequency Support Prediction

After the discussion of group sparsity, the algorithm of DCS based on mobility patterns is demonstrated in this sub-section. DCS processes the estimation by a time-varying observation process, that is to obtain a recursive solution that improves the accuracy of simple CS by using the prior information. In consideration of the scenario described in Section II, the methods based on the history observation only are not suitable. And the accuracy improvement of the iterative support prediction has been proven in [47] and [48]. Therefore, the support prediction based on temporal varying rules of space and frequency domains relation has been proposed, and its prior information results from history estimation, mobility patterns, and current observation. Among the traffic regulations, the velocity limitation is the most stable, universal, and accessible mobility pattern [12], so it is employed as an example in this paper to illustrate the idea.

For a specific mobile transmitter, just like the depiction in Fig. 2, the history information of its position can be utilized to indicate the possible positions of the future, e.g., the hollow dots within the dashed circle are the possible positions of the future for the exact mobile transmitter. Thus, according to the

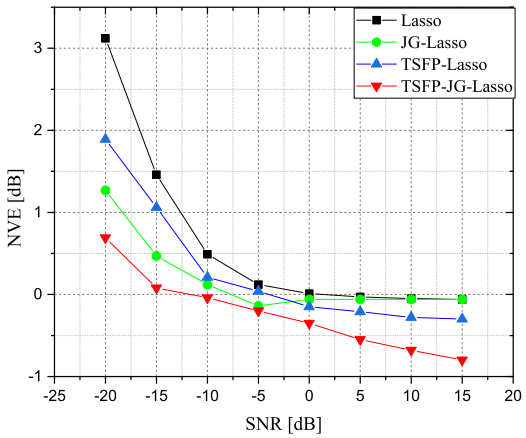

Fig. 5. NVEs versus SNRs with different methods $\alpha(t)$.

velocity limitation (i.e., information from mobility patterns), the support stemming from spatial variance (or invariance) can be defined as

$$\Delta_{spa} := \left\{ \begin{array}{c} i | i = (q-1) \times N_p + p, \hat{\varsigma}_{p'q}(t-\tau) > 0, \\ p' \in \mathbb{P}, \| s_p - s_{p'} \|_2^2 \leq v_{limit} \cdot \tau \end{array} \right\}, \tag{10}$$

where τ is the time interval, $\hat{\varsigma}_{p'q}(t-\tau)$ is entry of BEM coefficients estimation at time slot $t-\tau$, and $\mathbb{P} := \{p | p \in [1, N_p], p \in \mathbb{Z}^+\}$.

Next, we discuss the frequency predictive support based on the history estimation. Since a mobile transmitter's emitting frequency band can be measured by sensors, its variation is known to the regional CR. And the support results from frequency invariance can be defined as

$$\Delta_{freq} := \left\{ \begin{array}{c} i | i = (q-1) \times N_p + p, \hat{\varsigma}_{p'q}(t-\tau) > 0, \\ p' \in \mathbb{P}, q \in \mathbb{Q}, p = 1, 2, \cdots, N_p \end{array} \right\}, \tag{11}$$

where $\mathbb{Q} := \{q | q \in [1, N_q], q \in \mathbb{Z}^+\}$.

Then, to reduce the influence of noise, the current independent estimation pre-result also helps modify the predictive support of $\hat{\varsigma}(t)$. And it can be obtained by minimizing the loss function mentioned in (6) based on current measurements $\mathbf{\Phi}(t)$. And the support of pre-result is denoted as

$$\Delta_{current} := \{ i | i = (q-1) \times N_p + p, \check{\varsigma}_{pq}(t) > 0 \}, \tag{12}$$

where $\check{\varsigma}_{pq}(t)$ denotes the entry of pre-estimation based on current collection of measurements.

Since these three supports indicate the possible non-zero entries from different prior information, their intersection is the predictive support, which can be denoted as

$$\Delta_{pred} = \Delta_{freq} \cap \Delta_{spa} \cap \Delta_{current}. \tag{13}$$

After the solution of the predictive support, we could compute the estimation of $\varsigma(t)$ at each time slot t while setting all other values to zero. The simple LS on known support can obtain the distribution of PSD along with the precise support of $\varsigma(t)$ [39], but the predictive support is obtained based on the history and current information to indicate the possible nonzero entries, which means $\varsigma(t)$ within the predictive support is still sparse. So, the Lasso is chosen for the last estimation instead of common nonnegative LS, which can be expressed as

$$\min_{\varsigma_{\Delta_{pred}} \geq 0} \left\| \mathbf{\Phi}(t) - \mathbf{B}^{\Delta_{pred}} \cdot \varsigma_{\Delta_{pred}}(t) - \sigma_m^2 \cdot \mathbf{1}_{N_m N_l \times 1} \right\|^2 + \lambda_{\Delta_{pred}} \left\| \varsigma_{\Delta_{pred}}(t) \right\|_1, \tag{14}$$

where $\mathbf{B}^{\Delta_{pred}}$ denotes the Δ_{pred} columns of $\mathbf{B}$, $\varsigma_{\Delta_{pred}}(t)$ denotes the Δ_{pred} entries of $\varsigma(t)$, and other entries are setting as zero

$$\varsigma_{\Delta_{pred}^C}(t) = \mathbf{0}_{N_{pred}^C \times 1}, \tag{15}$$

where Δ_{pred}^C denotes the complement of Δ_{pred} and N_{pred}^C denotes the number of Δ_{pred}^C entries. And $\{\varsigma_{TSFP}(t)\}_{t=1}^{toT}$ equals $\{\hat{\varsigma}(t)\}_{t=1}^{toT}$ of (14) and (15).

The algorithm TSFP-Lasso on the support of expansion coefficients is illustrated in **Algorithm 2**.

Algorithm 2 TSFP-Lasso on the support of expansion coefficients estimation

Input: $\{s_p\}_{p=1}^{Np}, \{\beta_q(f)\}_{q=1}^{N_q}, \{s_m\}_{m=1}^{N_m}, \{f_l\}_{l=1}^{N_l}, \{\mathbf{\Phi}(t)\}_{t=1}^{toT}, v_{limit}$
Parameters: $\eta, d_{res}, \lambda, \lambda_{T_{pred}}$
if $t = 1$ **do**
  Obtain $\varsigma(t)$ by Lasso using (7)
end if
for $t = 2, 3, \cdots, toT$ **do**
  Update Δ_{pred} using (10)-(13)
  if $\Delta_{pred} \neq \oslash$ **do**
    Obtain $\hat{\varsigma}(t)$ using (13)
  else
    Obtain $\hat{\varsigma}(t)$ using (7)
  end if
end for
$\{\varsigma_{TSFP}(t)\}_{t=1}^{toT}$ equals $\{\hat{\varsigma}(t)\}_{t=1}^{toT}$
Output: $\{\varsigma_{TSFP}(t)\}_{t=1}^{toT}$

C. Joint Group-Lasso of Temporal Space-frequency Support Prediction

Finally, the Lasso part of TSFP-Lasso can be replaced by JG-Lasso to exploit the different sparsity in space and frequency domains, named as TSFP-JG-Lasso. The estimation steps of TSFP-JG-Lasso are similar to TSFP-Lasso, except for the estimation of pre-result. Although TSFP-JG-Lasso has the capability to utilize temporal space-frequency support prediction information to improve accuracy, this feature is not obligatory. In other words, when temporal space-frequency information is unavailable, TSFP-JG-Lasso can still function as JG-Lasso. This demonstrates the flexibility of the method. And steps of TSFP-JG-Lasso are illustrated in **Algorithm 3** in detail.

Algorithm 3 TSFP-JG-Lasso on the support of expansion coefficients estimation

Input: $\{s_p\}_{p=1}^{Np}, \{\beta_q(f)\}_{q=1}^{N_q}, \{s_m\}_{m=1}^{N_m}, \{f_l\}_{l=1}^{N_l}, \{\mathbf{\Phi}(t)\}_{t=1}^{toT}, v_{limit}$
Parameters: $\eta, d_{res}, \lambda_{spa}, \lambda_{freq}, \lambda_{T_{pred}}$
if $t = 1$ **do**
  Obtain $\varsigma(t)$ by JG-Lasso using (9)
end if
for $t = 2, 3, \cdots, toT$ **do**
  Update Δ_{pred} using (10)-(13)
  if $\Delta_{pred} \neq \oslash$ **do**
    Obtain $\hat{\varsigma}(t)$ using (15)
  else
    Obtain $\hat{\varsigma}(t)$ using (7)
  end if
end for
$\{\varsigma_{TSFP-JG}(t)\}_{t=1}^{toT}$ equals $\{\hat{\varsigma}(t)\}_{t=1}^{toT}$
Output: $\{\varsigma_{TSFP-JG}(t)\}_{t=1}^{toT}$

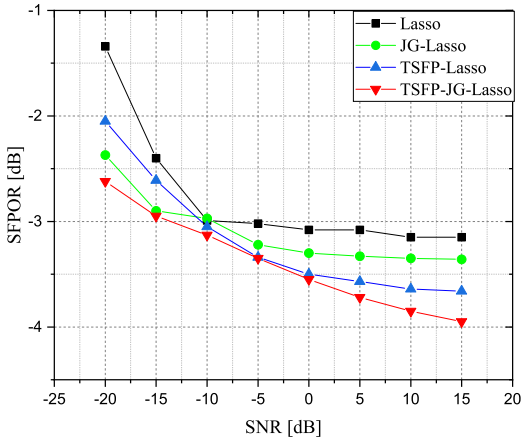

Fig. 6. SFPORs versus SNRs with different methods $\alpha(t)$.

IV. Simulation Results and Performance Analysis

A. Numerical Experiments Setup

To quantify the estimation performance of each method, two evaluation metrices have been chosen for the analysis comparing Lasso, JG-Lasso, TSFP-Lasso and TSFP-JG-Lasso. One is the NVE, which is utilized to compare the l_1-norm of difference between true values and estimations, defined as

$$\mathrm{NVE} := \frac{1}{toT}\sum_{t=1}^{toT} 10\log_{10}\left(\frac{\|\hat{\varsigma}(t)-\varsigma(t)\|_1}{\|\varsigma(t)\|_1}\right)[\mathrm{dB}]. \quad (16)$$

Another is the SFPOR, which is applied to compare the spatial- frequency difference between true values and estimations, better describing the power distribution along space and frequency domains, defined as

$$\mathrm{SFPOR} := \frac{1}{toT}\sum_{t=1}^{toT} 10\log_{10}\sum_{p=1}^{N_p}\sum_{q=1}^{N_q}(\cdot)[\mathrm{dB}], \quad (17)$$

where $(\cdot) = \frac{\hat{\alpha}_{pq}(t)-\alpha_{pq}(t)}{(\min\|p-p^\dagger\|+1)\times(\min\|q-q^\dagger\|+1)}$, $\alpha_{pq}(t)$ is the (p,q)th entry element of the matrix $\alpha(t)$, $p^\dagger$ and $q^\dagger$ are the serial set of nonzero values in $\alpha(t)$. The numerator of $(\cdot)$ represents the individual coefficient difference between true value and estimation on each spatial point, in each frequency band and at each time slot while the dominator represents the product of spatial difference and frequency band difference.

The setup of Monte Carlo simulation includes $N_p = 36$ possible spatial positions, $N_q = 8$ known expansion bases, $N_m = 6$ sensors collecting signals which scan $N_l = 42$ frequencies from 15 to 30 MHz, reference distance $d_{ref} = 10$ m, velocity limitation $v_{limit} = d_{ref}/\tau$, and three mobile transmitters are set within the region of interest. In consideration of universality, their signal emitting powers are different from each other and their working frequency bands are also nonoverlapping. Furthermore, these mobile transmitters have distinct-different movement rules. One is that transmitters move in different directions which means the distances between each other vary with time lapse. Another is one of them always keep moving while others stay at the same position randomly. These diverse movement rules facilitate the experimental completeness.

B. Performance Analysis

It shows in Fig. 5 that the NVE of each method versus different signal noise ratio (SNR). It can be seen that all NVEs decrease with the SNR, and the NVE of Lasso is always highest while those of other methods are low, which indicates both joint group-Lasso and temporal space-frequency support prediction have less estimation error, for they exploit the sparsity of BEM coefficients better than Lasso. Meanwhile, the difference of Lasso between other methods declines with the SNR except TSFP-JG-Lasso, which indicates those methods perform better on the condition of lower SNR than Lasso. That is because the joint group-Lasso and temporal support prediction can reduce noise interference, which increase the estimation accuracy.

Also, the NVE of JG-Lasso is higher than that of TSFP-Lasso when SNR is lower 0 dB but lower when SNR is higher than 0 dB. This phenomenon demonstrates that the exploitation of group sparsity contributes more than the utilization of mobility pattern to the accurate estimation on the condition of low SNR while the utilization of mobility pattern is superior to group sparsity exploitation on the condition of higher SNR.

Moreover, the NVE of JG-Lasso is similar with that of Lasso when SNR is higher than 5 dB, while the superiority of TSFP-Lasso over Lasso is maintained across varying SNRs. This can be attributed to JG-Lasso's superior ability to reduce the impact of noise on Lasso, which becomes more evident in low SNR scenarios due to its multi-domain sparsity analysis. However, as the SNR increases, the advantage of JG-Lasso may not be significant, resulting in similar NVE values for both methods. This phenomenon illustrates that the exploitation of group sparsity has better performance on the condition of low SNR. And it can also be suggested from the Fig. 5 that

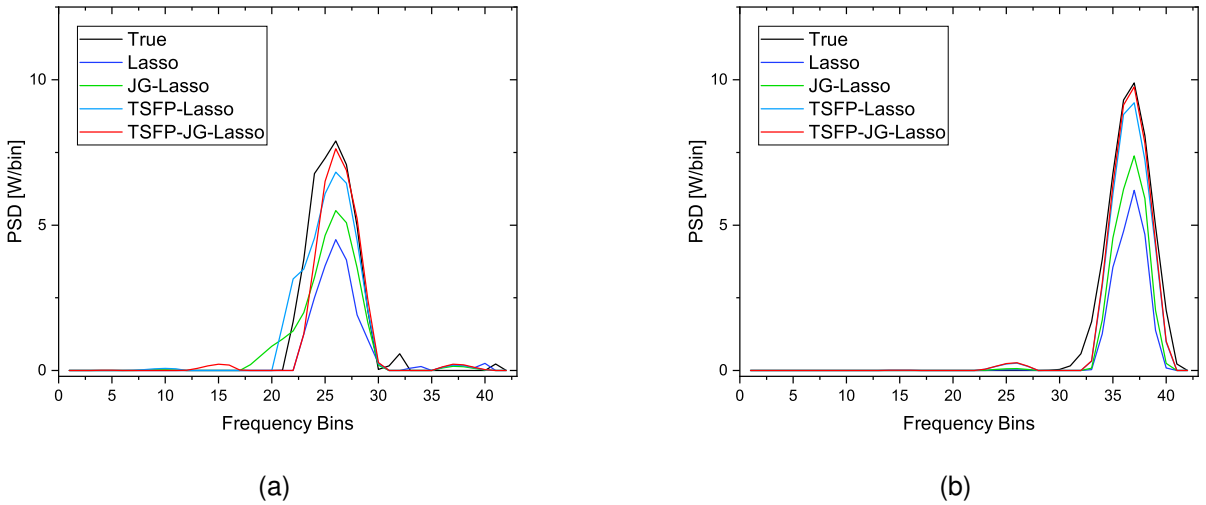

Fig. 7. The examples of PSD charts of No. 2 and No. 3 transmitters. (a) No. 2. (b) No. 3.

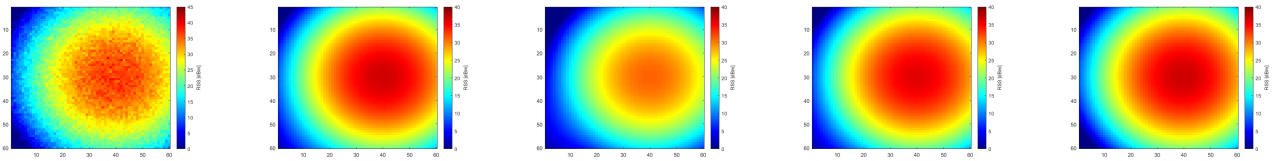

Fig. 8. Radio maps at 14th frequency bin and a specific time slot with $N_l = 42$ when SNR equals 0 dB. (a) True value. (b) Lasso estimation. (c) JG-Lasso estimation. (d) TSFP-Lasso estimation. (e) TSFP-JG-Lasso estimation.

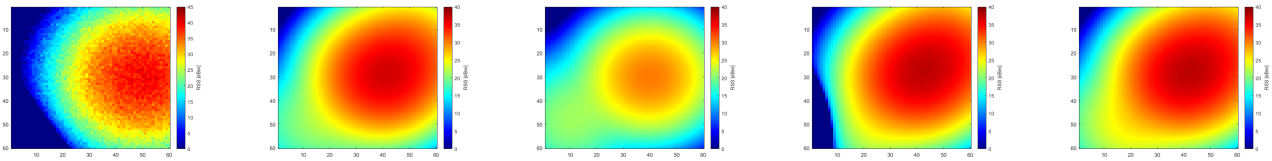

Fig. 9. Radio maps at 25th frequency bin and a specific time slot with $N_l = 42$ when SNR equals 0 dB. (a) True value. (b) Lasso estimation. (c) JG-Lasso estimation. (d) TSFP-Lasso estimation. (e) TSFP-JG-Lasso estimation.

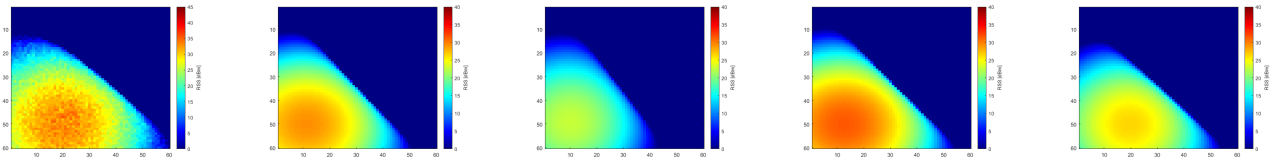

Fig. 10. Radio maps at 33th frequency bin and a specific time slot with $N_l = 42$ when SNR equals 0 dB. (a) True value. (b) Lasso estimation. (c) JG-Lasso estimation. (d) TSFP-Lasso estimation. (e) TSFP-JG-Lasso estimation.

TSFP-JG-Lasso is superior to others because its lowest NVE along all methods.

As for Fig. 6, SFPORs of different methods are depicted to describe the power distribution in spatial and frequency domain. Similar with NVEs, SFPORs decrease with the growth of SNR. But the difference between SFPOR of JG-Lasso and TSFP-Lasso is larger than NVEs of them, which demonstrates the utilization of mobility patterns contributes to the estimation accuracy based on different sparse patterns and temporal varying rules of space and frequency domains. Also,

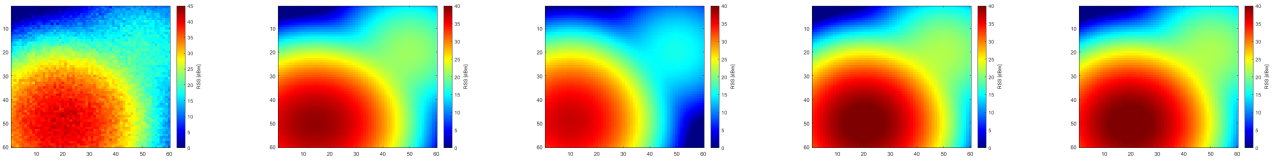

Fig. 11. Radio maps at 36th frequency bin and a specific time slot with $N_l = 42$ when SNR equals 0 dB. (a) True value. (b) Lasso estimation. (c) JG-Lasso estimation. (d) TSFP-Lasso estimation. (e) TSFP-JG-Lasso estimation.

the superiority of JG-Lasso and TSFP-Lasso to each other on the condition of different SNRs can be demonstrated in Fig. 6, similar with that in Fig. 5.

And SFPORs can better help discriminate the estimation accuracy of these methods than NVEs because of the lager difference, especially for the Lasso and JG-Lasso when SNR is higher than 5 dB. In addition, TSFP-JG-Lasso is still the most accurate estimation method due to its lowest SFPORs, which exploits the sparse patterns difference between space and frequency domains and predicts the support according to the mobility patterns as the prior information meanwhile. The PSD charts of different mobile transmitters' locations at a specific time slot are displayed in Fig. 7, and No. 2 and No. 3 transmitter is displayed in Fig. 7(a) and 7(b), respectively.

Figs. 8, 9, 10, and 11 compare true values and estimation results of radio maps at the 14th, 25th, 33th, and 36th frequency bin, respectively, and SNR is set as 0 dB. Also, among these frequency bins, 14th, 25th, and 36th is the central frequency bin of No. 1, No. 2 and No. 3 mobile transmitters, respectively. From these figures, radio maps of Lasso can shed light on basic outlines of true values at different frequency bins, but RSS distribution of JG-Lasso is more explicit to describe transmitter's location while transmitter's emitting power estimations of TSFP-Lasso are closer to true values. To sum up, TSFP-JG-Lasso are superior to other methods in accuracy because their profiles are the most similar with true values.

V. Conclusion

A novel DCS framework by using multiple domains information has been propounded for PSD maps construction according to the sparse patterns difference between space and frequency domains as well as temporal varying rules in this paper. The proposed framework utilizes history estimation information and transmitters' mobile patterns to obtain temporal varying rules of space and frequency domains, which contributes to DCS support prediction. Meanwhile, it employs joint group-Lasso with different plenty items based on different sparse patterns. Furthermore, it is also able to adjust construction methods flexibly to construct PSD maps in allusion to possible absence of history information or mobility patterns. The experimental results have proven the framework's effectiveness and TSFP-JG-Lasso's superiority in accuracy.

References

[1] H. Idsoe, M. Hamid, T. Jordbru, L. R. Cenkeramaddi, and B. Beferull-Lozano, "Spectrum cartography using adaptive radial basis functions: Experimental validation," in *Proc. IEEE SPAWC*, 2017.

[2] G. Zhang, X. Fu, J. Wang, X. L. Zhao, and M. Hong, "Spectrum cartography via coupled block-term tensor decomposition," *IEEE Trans. Signal Process.*, vol. 68, pp. 3660–3675, 2020.

[3] H. Yilmaz Birkan, T. Tugcu, F. Alagöz, and S. Bayhan, "Radio environment map as enabler for practical cognitive radio networks," *IEEE Commun. Mag.*, vol. 51, no. 12, pp. 162–169, 2013.

[4] Y. S. Reddy, A. Kumar, O. J. Pandey, and L. R. Cenkeramaddi, "Spectrum cartography techniques, challenges, opportunities, and applications: A survey," *Pervasive and Mobile Computing*, vol. 79, pp. 101511, 2022.

[5] Y. Teganya and D. Romero, "Deep completion autoencoders for radio map estimation," *IEEE Trans. Wireless Commun.*, vol. 21, no. 3, pp. 1710–1724, 2022.

[6] M. Pesko, T. Javornik, A. Košir, M. Štular, and M. Mohorčič, "Radio environment maps: The survey of construction methods," *KSII Trans. Internet and Information Systems*, vol. 8, no. 11, pp. 3789–3809, 2014.

[7] M. Joneidi, H. Yazdani, A. Vosoughi, and N. Rahnavard, "Source localization and tracking for dynamic radio cartography using directional antennas," in *Proc. IEEE SECON*, 2019.

[8] S. Shrestha, X. Fu, and M. Hong, "Deep spectrum cartography: Completing radio map tensors using learned neural models," *IEEE Trans. Signal Process.*, vol. 70, pp. 1170–1184, 2022.

[9] J. Bazerque, "Leveraging sparsity for genetic and wireless cognitive networks," Ph.D. dissertation, 2013. [Online]. Available: http://conservancy.umn.edu/handle/11299/157612

[10] Y. Teganya and D. Romero, "Data-driven spectrum cartography via deep completion autoencoders," in *Proc. IEEE ICC*, 2020.

[11] M. Suchański, P. Kaniewski, J. Romanik, E. Golan, and K. Zubel, "Radio environment maps for military cognitive networks: Density of small-scale sensor network vs. map quality," *Eurasip J. Wireless Commun. Netw.*, vol. 2020, no. 1, 2020.

[12] M. N. Ahangar, Q. Z. Ahmed, F. A. Khan, and M. Hafeez, "A survey of autonomous vehicles: Enabling communication technologies and challenges," *Sensors*, vol. 21, no. 3, pp. 1–33, 2021.

[13] B. Yang *et al.*, "Edge intelligence for autonomous driving in 6G wireless system: Design challenges and solutions," *IEEE Wireless Commun.*, vol. 28, no. 2, pp. 40–47, 2021.

[14] Z. Wei, R. Yao, J. Kang, X. Chen, and H. Wu, "Three-dimensional spectrum occupancy measurement using UAV: Performance analysis and algorithm design," *IEEE Sensors J.*, vol. 22, no. 9, pp. 9146–9157, 2022.

[15] J. M Lebreton, N. Murad, and R. Lorion, "Radio frequency mapping using an autonomous robot: Application to the 2.4 GHz band," *IOP Conference Series: Materials Science and Engineering*, vol. 120, no. 1, p. 12001, 2016.

[16] G. Boccolini, G. Hernandez-Penaloza, and B. Beferull-Lozano, "Wireless sensor network for spectrum cartography based on Kriging interpolation," in *Proc. IEEE PIMRC*, 2012.

[17] H. Xia, S. Zha, J. Huang, and J. Liu, "Radio environment map construction by adaptive ordinary Kriging algorithm based on affinity propagation clustering," *International J. Distributed Sensor Networks*, vol. 16, no. 5, 2020.

[18] Y. Q. Xu *et al.*, "Radio environment map construction based on spatial statistics and Bayesian hierarchical model," *IEEE Trans. Cog. Commun. Netw.*, vol. 7, no. 3, pp. 767–779, 2021.

[19] D. Romero, S. J. Kim, and G. B. Giannakis, "Stochastic semiparametric regression for spectrum cartography," in *Proc. IEEE CAMSAP*, 2015.

[20] G. Ding *et al.*, "Cellular-base-station assisted device-to-device communications in TV white space," *IEEE J. Sel. Areas Commun.*, vol. 34, no. 1, pp. 107–121, 2016.

[21] J. Bazerque and G. Giannakis, "Nonparametric basis pursuit via sparse kernel-based learning," *IEEE Signal Process. Mag.*, vol. 30, no. 4, pp. 112–125, 2013.

[22] C. Garcia-Cardona and B. Wohlberg, "Convolutional dictionary learning: A comparative review and new algorithms," *IEEE Trans. Comput. Imag.*, vol. 4, no. 3, pp. 366–381, 2018.

[23] B. A. Jayawickrama, E. Dutkiewicz, I. Oppermann, G. Fang, and J. Ding, "Improved performance of spectrum cartography based on compressive sensing in cognitive radio networks," in *Proc. IEEE ICC*, 2013.

[24] B. Jayawickrama, E. Dutkiewicz, I. Oppermann, and M. Mueck, "Iteratively reweighted compressive sensing based algorithm for spectrum cartography in cognitive radio networks," in *Proc. WCNC*, 2014.

[25] E. J. Candès, J. Romberg, and T. Tao, "Robust uncertainty principles: Exact signal frequency information," *IEEE Trans. Inf. Theory*, vol. 52, no. 2, pp. 489–509, 2006.

[26] D. L. Donoho, "Compressed sensing," *IEEE Trans. Inf. Theory*, vol. 52, no. 4, pp. 1289–1306, 2006.

[27] Robert and Tibshirani, "Regression shrinkage and selection via the Lasso," *J. the Royal Statistical Society. Series B (Methodological)*, 1996.

[28] S. Foucart, "The sparsity of LASSO-type minimizers," *Applied and Computational Harmonic Analysis*, vol. 62, pp. 441–452, 2023.

[29] G. B. Giannakis and C. Tepedelenlioğlu, "Basis expansion models and diversity techniques for blind identification and equalization of time-varying channels," *Proc. IEEE*, vol. 86, no. 10, pp. 1969–1986, 1998.

[30] L. Deng, Z. Chen, and Y. Zhao, "Basis expansion model for channel estimation in LTE-R communication system," *Digital Commun. Netw.*, vol. 2, no. 2, pp. 92–96, 2016.

[31] J.-A. Bazerque and G. B. Giannakis, "Distributed spectrum sensing for cognitive radios by exploiting sparsity," in *Asilomar Conference on Signals, Systems and Computers*, 2008.

[32] J. A. Bazerque and G. B. Giannakis, "Distributed spectrum sensing for cognitive radio networks by exploiting sparsity," *IEEE Trans. Signal Process.*, vol. 58, no. 3 PART 2, pp. 1847–1862, 2010.

[33] M. Yuan and Y. Lin, "Model selection and estimation in additive regression models," *J. the Royal Statistical Society. Series B (Methodological)*, vol. 68, no. 1, pp. 49–67, 2006.

[34] J. A. Bazerque, G. Mateos, and G. B. Giannakis, "Group-Lasso on splines for spectrum cartography," *IEEE Trans. Signal Process.*, vol. 59, no. 10, pp. 4648–4663, 2011.

[35] J. Bazerque, G. Mateos, and G. B. Giannakis, "Basis pursuit for spectrum cartography," in *Proc. IEEE ICASSP*, 2011.

[36] N. Vaswani and J. Zhan, "Recursive recovery of sparse signal sequences from compressive measurements: A review," *IEEE Trans. Signal Process.*, vol. 64, no. 13, pp. 3523–3549, 2016.

[37] S. D. Babacan, R. Molina, and A. K. Katsaggelos, "Bayesian compressive sensing using laplace priors," *IEEE Trans. Image Process.*, vol. 19, no. 1, pp. 53–63, 2010.

[38] D. Sejdinović, C. Andrieu, and R. Piechocki, "Bayesian sequential compressed sensing in sparse dynamical systems," 2010.

[39] N. Vaswani, "LS-CS-residual (LS-CS): Compressive sensing on least squares residual," *IEEE Trans. Signal Process.*, vol. 58, no. 8, pp. 4108–4120, 2010.

[40] N. Vaswani, "KF-CS: Compressive sensing on kalman filtered residual," *Eprint Arxiv*, 2009.

[41] N. Vaswani and W. Lu, "Modified-CS: Modifying compressive sensing for problems with partially known support," *IEEE Trans. Signal Process.*, vol. 58, no. 9, pp. 4595–4607, 2010.

[42] S. Vladimir and S. Cheng, "Compressive image sampling with side information," in *Proc. IEEE ICIP*, 2009.

[43] M. E. Tipping and A. C. Faul, "Fast marginal likelihood ,aximisation for sparse Bayesian models," in *Proc. Ninth International Workshop on Artificial Intelligence & Statistics*, 2003.

[44] S. S. Chen and D. Saunders, "Atomic decomposition by basis pursuit," *Siam Review*, vol. 43, no. 1, pp. 129–159, 2001.

[45] A. E. Hoerl and R. W. Kennard, "Ridge regression: Biased estimation for nonorthogonal problems," *Technometrics A J. Stats for the Physical Chemical & Engineering ences*, vol. 42, 2000.

[46] J. E. Vogt and V. Roth, "A complete analysis of the $l_{1,p}$ group-Lasso," in *Proc. ICML*, 2012.

[47] R. E. Carrillo, L. F. Polania, and K. E. Barner, "Iterative algorithms for compressed sensing with partially known support," in *Proc. IEEE ICASSP*, 2010.

[48] Y. Wang and W. Yin, "Sparse signal reconstruction via iterative support detection," *SIAM J. Imaging Sciences*, vol. 3, no. 3, pp. 462–491, 2010.

Haiyang Xia received the B.E. degree in Electronic Engineering and M.S. degrees in Electronic Science and Technology from the College of Electronic Science and Technology, National University of Defense Technology (NUDT), Changsha, China, in 2015 and 2020, respectively. He is currently working toward his Ph.D. degree with the College of Electronic Science and Technology, NUDT. His research interests include radio environment map construction, cognitive radio, and radio spectrum sensing and management.

Song Zha received the M. S. degree in Signal and Information Processing from the Electronic Engineering Institute (EEI) and Ph.D. degree in Electronic Science and Technology from the National University of Defense Technology (NUDT), in 2010 and 2014, respectively. He is currently a Lecturer in NUDT. His research interests include electromagnetic environment sensing and electromagnetic compatibility.

Jijun Huang received the M.S degree in Electromagnetic Field and Microwave Technologies and the Ph.D. degree in Electronic Science and Technology from the National University of Defense Technology (NUDT), in 1997, and 2005, respectively. He is currently an Associate Professor in NUDT. His current research interests include spectrum management and electromagnetic resource optimization.

Jibin Liu received the M.S degree in Electromagnetic Field and Microwave Technologies and the Ph.D. degree in Electronic Science and Technology from the National University of Defense Technology (NUDT), in 1998, and 2007, respectively. He is currently a full Professor with the school of Electronic Science and Technology at NUDT. His current research interests include spectrum management, electromagnetic compatibility and RF front-end electromagnetic protection.

Peiguo Liu received the B.S. and M.S. degrees in Electromagnetic Field and Microwave Technologies and the Ph.D. degree in Communication and Information Systems from the National University of Defense Technology (NUDT), Changsha, China, in 1990, 1994, and 2000, respectively. From 2004 to 2005, he was a Visiting Scholar with the University of Calgary, Calgary, AB, Canada. He is currently a Professor with NUDT. His current research interests include electromagnetic radiation, electromagnetic compatibility and protection.